MACSima Imaging Cyclic Staining (MICS) Technology Reveals Combinatorial Target Pairs for CAR T Treatment of Solid Tumors

Ali Kinkhabwala
Miltenyi Biotec B.V. & Co. KG
Christoph Herbel
Miltenyi Biotec B.V. & Co. KG
Jennifer Pankratz
Miltenyi Biotec B.V. & Co. KG
Dmytro Yushchenko
Miltenyi Biotec B.V. & Co. KG
Silvia Rüberg
Miltenyi Biotec B.V. & Co. KG
Paurush Praveen
Miltenyi Biotec B.V. & Co. KG
Sandy Reiß
Miltenyi Biotec B.V. & Co. KG
Federico Rodriguez
Miltenyi Biotec B.V. & Co. KG
Daniel Schäfer
Miltenyi Biotec B.V. & Co. KG
Jutta Kollet
Miltenyi Biotec B.V. & Co. KG
Vera Dittmer
Miltenyi Biotec B.V. & Co. KG
Manuel Martinez-Osuna
Miltenyi Biotec B.V. & Co. KG
Lara Minnerup
Miltenyi Biotec B.V. & Co. KG
Claudia Reinhard
Miltenyi Biotec B.V. & Co. KG
Andrzej Dzionek
Miltenyi Biotec B.V. & Co. KG
Stefan Borbe

Miltenyi Biotec B.V. & Co. KG
Thomas Rockel
Miltenyi Biotec B.V. & Co. KG
Martin Buescher
Miltenyi Biotec B.V. & Co. KG
Jürgen Krieg
Miltenyi Biotec B.V. & Co. KG
Michel Nederlof
Qi Biotech, Inc.
Melanie Jungblut
Miltenyi Biotec B.V. & Co. KG
Dominik Eckardt
Miltenyi Biotec B.V. & Co. KG
Olaf Hardt
Miltenyi Biotec B.V. & Co. KG
Christian Dose
Miltenyi Biotec B.V. & Co. KG
Eik Schumann
Miltenyi Biotec B.V. & Co. KG
Ralf-Peter Peters
Miltenyi Biotec B.V. & Co. KG
Stefan Miltenyi
Miltenyi Biotec B.V. & Co. KG
Jürgen Schmitz
Miltenyi Biotec B.V. & Co. KG
Werner Müller
Miltenyi Biotec B.V. & Co. KG
Andreas Bosio (andreasbo@miltenyi.com)
Miltenyi Biotec B.V. & Co. KG

Research Article

Keywords: single cell, MICS (MACSimaTM Imaging Cyclic Staining), immunofluorescent, photobleaching

Posted Date: August 20th, 2021

DOI: https://doi.org/10.21203/rs.3.rs-825947/v1

Abstract

Many critical advances in research utilize techniques that combine high-resolution with high-content characterization at the single cell level. We introduce the MICS (MACSima^{TM} Imaging Cyclic Staining) technology, which enables the immunofluorescent imaging of hundreds of protein targets across a single specimen at sub-cellular resolution. MICS is based on cycles of staining, imaging, and erasure, using photobleaching of fluorescent labels of recombinant antibodies (REAfinity^{TM}), release of antibodies (REAlease^{TM}) or their labels (REAdyelease^{TM}). Multimarker analysis can identify potential targets for immune therapy against solid tumors. With MICS we analysed human glioblastoma, ovarian and pancreatic carcinoma, and 16 normal tissues. One potential target pair for chimeric antigen receptor (CAR) T-cell therapies identified for ovarian carcinoma is EPCAM/THY1. Using an adapter CAR T cell approach, we show selective killing of cells only in presence of both markers. MICS represents a new high content microscopy methodology to be widely used for personalized medicine.

Introduction

Analysis of cancer cell diversity and immune contexture is of high relevance for tumor subclassification and the development of novel targeted immunotherapies. The analysis can be improved by new multiplexing technologies using either optical or mass spectrometric readouts such as multi-epitope-ligand cartography (MELC)[1], ChipCytometry[2], mass cytometry[3], multiplexed ion beam imaging (MIBI)[4], cyclic immunofluorescence (CycIF)[5], multiplex immunohistochemistry[6], co-detection by indexing (CODEX)[7], or InSituPlex[8]. However, there are still limitations in spatial resolution, degree of binder-based multiplexing, and tissue integrity. Transition element isotopes chelated to antibodies as used in mass spectrometric readouts are confined to about 40 unique labels[3]. Antibody-oligonucleotide conjugates used for cyclic immunofluorescence analysis need to be carefully selected limiting these technologies to roughly 60 analytes[9].

CAR T cell–based therapies have resulted in a remarkable success in the treatment of hematopoietic malignancies[10], but have not yet led to a breakthrough in solid tumors. Besides inherent obstacles presented by the tissue microenvironment that can hamper T cell infiltration, there is also a lack of cell surface target molecules that are suitable for CAR T cells, i.e. high coverage of tumor cells and low on-target/off-tumor toxicity. A number of cell surface markers are currently investigated for CAR T cell therapy in solid tumors[11] and strategies have been outlined to combine different markers to circumvent tumor escape mechanisms (“OR” gated combinatorial CARs) or to reduce off tumor toxicity (“AND” gated CARs)[12].

We describe a novel imaging system for fully automated cyclic immunofluorescence analysis including a mechanism for most gentle erasure of signal with the potential to apply hundreds of binders to a single specimen. Based on a new image processing pipeline for robust removal of imaging artifact, we demonstrate highly sensitive detection of cellular proteins at subcellular resolution allowing a deep

insight into basic scientific questions such as the comprehensive identification and quantification of cellular subtypes of the spleen or visualization of tumor heterogeneity. Applied to the screening of glioblastoma multiforme (GBM), high-grade serous ovarian carcinoma (HGSOC), and pancreatic ductal adenocarcinoma (PDAC), it reveals marker combinations with a preferable on-target/on-tumor vs on-target/off-tumor profile suitable for CAR T cell development. We validate the screening approach using adapter CAR T cells for an AND gated combinatorial targeting of cancer cells co-expressing EPCAM and THY1.

Results

Cyclic immunofluorescence staining with the MACSima™ Imaging System

The MACSima™ Imaging Platform (Fig. 1a) operates by iterative immunofluorescent staining, sample washing, multi-field imaging, and signal erasure (Fig. 1b), using three fluorochrome-conjugated antibodies per cycle (Fig. 1c). Standard and novel image processing algorithms were employed to remove imaging artifacts and to maximize signal-to-noise ratio. An in-depth analysis of the image stacks generated on the instrument was achieved using a novel software (Quantitative Imaging Systems) allowing to navigate through the images, segmenting images into single cells and clustering cells and proteins according to their profile across all cells (Fig. 1d). A liquid handling system was programmed to prepare the antibody conjugate staining solution, apply it to the biological sample, and washing following staining or release incubation steps. Images were obtained by a widefield microscope in an epifluorescence setup with a 20x or 2x objective using infrared, red, green, blue, and UV LEDs and filters. For signal erasure we first tested photobleaching of FITC, PE, and APC conjugated hybridoma or REAfinity™ antibodies, recombinantly engineered with the same human IgG1 backbone and without the need for FcR blocking (Fig. 1b, Fig S1a). Remaining signals were imaged separately and subtracted from the subsequent image. While photobleaching was efficient, it also prolonged the overall processing time, limited cyclic IF to the use of photo bleachable dyes and showed a tendency to slightly disrupt non-crosslinked specimen such as acetone fixated samples. Therefore, we developed a new type of binder-fluorochrome conjugates. Recombinantly engineered antibody fragments were generated, multimerized, fluorescently labelled and optimized to bind to epitopes on sections with high avidity. Disruption of the complex led either to the release of the fluorescent dye only (“REAdyelease”) (Fig S1b) or to the release of dye and binder fragment in case low epitope binding affinities were selected (“REAlease”) (Fig S1c). All three methods (photobleaching, REAdyelease, REAlease) for signal erasure could be used with combinations of binders with different fluorescent dyes applied in the same cycle of imaging (Fig S1d). We did not observe a limit on the number of IF cycles that could be applied to a single sample. Using formaldehyde-fixed paraffin-embedded (FFPE) or paraformaldehyde (PFA) fixed material, more than 300 unique antibodies could be applied to the same specimen. Based on systematic testing of antibody conjugates, we so far generated a library of about 1700 fluorochrome conjugates, covering roughly 300

distinct epitopes of biomolecules and qualified them for the analysis of human or mouse acetone-, PFA- or FFPE-fixed samples.

MICS analysis reveals a highly linear dynamic range over five orders of magnitude with a sensitivity down to a few proteins per cell

To determine the linearity and sensitivity of MICS and to compare with MACSQuant flow cytometry, we generated fluorescently labeled beads (Fig. 2a, inset) with distinct brightnesses by conjugation with different stoichiometries of fluorescent to dark labels. Image cytometry with the MACSima was significantly more sensitive for lower intensity beads (narrower shaded area in Fig. 2a), asymptoting to 9x better sensitivity (9x smaller standard deviation) for completely unlabeled beads. To compare sensitivities for cell-based targets, single-donor peripheral blood mononuclear cells (PBMCs) were measured. PBMCs were stained by different stoichiometric ratios of APC- and biotin- labeled CD3 antibodies (Fig. 2b). The intensity distributions of the stained vs non-stained cell subpopulations are plotted with estimated numbers of stained epitopes per cell (Fig. 2c) and individual histograms are depicted (Figs. 2d-g) (note the reference labels to these subpanels in Fig. 2c). To illustrate the discrimination power of the MACSima and MACSQuant, we report the separation parameter, s, for a double Gaussian fit where possible (Table 1). This parameter is defined as the difference in means of two populations divided by the square root of the sum of their individual variances[13] and is therefore a quantitative readout of the ability to resolve two different populations[14]. For the MACSQuant, a double-peaked population was still detectable for an average number of labeled epitopes of roughly 190 (s = 1.4, Fig. 2d). A second peak was still detectable (Figs. 2e,f) for the MACSima even down to roughly 19 labeled epitopes (s = 1.3, Fig. 2f), indicating that the MACSima is roughly 10x more sensitive. In addition, the distribution for the blank control was much narrower for the MACSima. Based on the ratio of the widths of the blank distributions, the MACSima was found to be 14.5x more sensitive than the MACSQuant (Fig. 2g), agreeing well with the factor of 10x obtained above from the separation parameter.

Table 1

Stoichiometric labeling percentages, average expected number of labeled CD3 proteins per cell[26], and separation parameters, *s*, for the MACSQuant and MACSima.

Labeling Percentage	Labeled CD3 Proteins Per Cell	MACSQuant Separation	MACSima Separation
100	57000	9.77	8.41
33.0	19000	9.19	9.62
10.0	5700	7.56	7.52
3.30	1900	5.11	4.78
1.00	570	2.87	2.76
0.330	190	1.41	2.29
0.100	57	n.a.	1.73
0.0330	19	n.a.	1.33
0.0100	5.7	n.a.	n.a.
0.00330	1.9	n.a.	n.a.
0.00100	0.57	n.a.	n.a.

The results shown in Fig. 2 for the linearity and sensitivity of the MACSima as compared to MACSQuant flow cytometry were acquired on the same reference sample to enable direct, unbiased comparison of both instruments, thereby providing a useful performance baseline for the MACSima. However, for a standard MICS run, additional corrections are applied in the full image processing pipeline (Fig. S2). These further improvements come primarily from the photobleaching of initial autofluorescence, the subtraction of remaining autofluorescence or residual staining from each new stained image, and the statistically optimal inference of individual pixel intensities for the generation of a high dynamic range (HDR) image (see Online Methods).

In depth analysis of mouse spleen tissue validates the performance of MICS and identifies at least 20 distinct cell types including rare cells with a frequency of 30–40 in 10000 cells

To demonstrate the power of the technology applied to tissue we performed a MICS analysis on a frozen section of a mouse spleen using 47 antibody markers spanning as many immune cells as possible. For this tissue, expression of key proteins and the cellular composition has been extensively characterized before[15]. Figure 3a shows the antibodies used for subsequent analyses. In Fig. 3b, expression levels of individual markers at single cell level obtained after segmentation were grouped using k-means

clustering. Four main groups of cell types were identified: T cells, B cells, Non-T and Non-B lymphocytes, and stroma cells. Within each group, subpopulations were identified, even at the level of rare cells. For example, 40 IgM Plasma cells and 38 CDa alpha/alpha positive T cells were found in the section consisting of 11996 cells (Fig S2). These cells can be found in the red pulp of the spleen next to the white pulp. To detect such rare cell populations from two separate cell linages in a complex cell population would be almost impossible in a single flow cytometry experiment. In Figs. 3c, d, and e, hierarchical clustering was used. The heatmap in Fig. 3c shows the main clusters. It is evident that even smaller clusters could be identified using higher cluster numbers and more sophisticated cluster methods. Figure 3d shows a map of the clusters joining similar cells to each other in a two-dimensional map. Figure 3e shows the expression of each marker of the clusters. In conclusion, the MICS technology can differentiate multiple cell populations in higher resolution and with special information in a single experiment that otherwise would require extensive flow cytometric analysis using multiple complex antibody marker mixes and gating strategies. The MICS technology can also be used for cell suspensions providing many markers with a better separation compared to multicolor flow cytometry.

MICS reveals novel pairs of surface proteins as candidates for CAR T based immune therapies

A second application of the MICS technology aims to find markers selectively expressed on solid tumor cells but not in normal tissue to develop cell based immune therapies. For this, we performed high-content expression analysis of proteins across several different tumor entities, i.e. GBM, HGSOC, and PDAC. First, GBM xenografts derived from primary tumors were analyzed for 371 cell surface markers by flow cytometry. 96 markers were selected according to the percentage of positive cells and their stain index (Table S1). Re-analyses on eight primary GBM by MICS showed the broadest and/or strongest expression for GD2, EGFR and cMET on tumor cells, but also a broad inter- and intratumor diversity (Figs. 4a, 6). To assess the respective toxicity profile, expression over 16 different human tissue samples (Figs. 5, S4, 6) was measured. We observed expression of GD2 in the brain (cerebellum, medulla oblongata), and a weak expression in healthy lung, pancreas, liver, ovary, skin, thyroid and testes tissues. EGFR was expressed in most healthy tissues and cMET primarily in pituitary glands, thyroid, lung, kidney, and heart. We compared the Pearson correlation coefficients for healthy and GBM samples with three marker pairs namely, GD2-EGFR, GD2-cMet and EGFR-cMet. The marker pair GD2-EGFR showed a stronger and significant correlation of up to 0.70 compared to all healthy brain tissue samples. For GD2-cMET and EGFR-cMET we found a higher correlation in non-GBM than GBM tissue. In conclusion, an AND gated combination of GD2 and EGFR suggests to be most promising for a CAR T cell based immunotherapy for GBM of the classical / mixed subtype[16].

Using a similar approach as described above, we previously reported the analysis of PDAC[17]. There, we identified CDCP1 (CD318), tetraspanin-8 (TSPAN8), cutaneous lymphocyte-associated antigen (CLA) and CECAM6 (CD66c) as target candidates for CAR T cell based immunotherapy. CDCP1 showed the most favorable pattern with almost no detectable protein expression in healthy tissues while e.g. TSPAN8 and CECAM6 raised safety concerns with respect to their expression in gastrointestinal and hematopoietic

tissues, respectively. We re-evaluated and extended the data by MICS, specifically aiming at identifying promissing target pairs (Figs. 4b, 5, S4, 6). After re-analyzing the co-expression of these markers, we concluded that an AND gated target combination of CDCP1 with TSPAN8 or CEACAM6 could be promising from a safety perspective of a CAR T cell therapy (Fig. 6), while development of CLA specific CAR T cells requires further technical solutions as it is expressed on activated CAR T cells[17]. Finally, we applied our screening approach to HGSOC. We found EPCAM being reliably expressed on all ovarian cancers showing a high coverage of cells in individual ovarian cancer samples (Figs. 4c, 6). As EPCAM is expressed on most epithelial cells, we searched for a second marker co-expressed on ovarian cancer cells, but not on non-cancerous epithelial cells. We identified THY1 with a characteristic expression on non-epithelial cells like fibroblasts (Fig. 4c) and co-expression with EPCAM on ovarian cancer cells (Fig. 4c). Over all tissues analyzed, we saw minor co-expression of EPCAM with THY1 on structures within kidney and breast tissue (Fig S4). The HGSOC samples showed a weak but significant correlation for cellular co-expression of EpCAM and THY1 while on healthy tissue e we observed only for breast a comparatively higher correlation, however, on a very low expression level (Fig. 6). In summary, MICS screening across multiple markers allowed us to identify marker pairs which could potentially be used to specifically eradicate tumor cells while not harming non-tumor cells in an AND gated application of CAR T cells.

Adapter CAR T cells allow to combine pairs of tumor markers for an AND gated specific killing of tumor cells

After having identified marker pairs for GBM, PDAC, and HGSOC, we considered adapter CAR T cells as an attractive system for multi-targeting of cancer cells. Here, CAR T cells are directed against a tag moiety, i.e. biotin, and, consequently, the targeting of the CAR T cells to the respective cancer cells is achieved via the addition of adapter molecules such as biotinylated antibodies, Fabs, or other antibody fragments. Adapter molecules can quickly be exchanged, differentially dosed, and removed from the system allowing dynamic interactions[18,19]. To test one of the identified candidate pairs, we generated ovarian cancer cells co-expressing EPCAM and THY1 in combination with eGFP. We performed in vitro CAR T cell functionality testing on these cells by titrating varying doses of biotinylated anti-EPCAM (Fig. S3a) and anti-THY1 (Fig. S3b) antibodies in the presence of adapter CAR T cells. These co-culture assays revealed defined ranges of antibody concentrations that initiate CAR T cell activation indicated by target cell lysis. Noteworthy, the combined usage of antibodies at concentrations which -used on their own- are too low to cause CAR T cell mediated target cell lysis (Fig. 4d and Fig. S3c) can trigger target cell lysis. Thus, adapter molecules at suboptimal doses for single targeting approaches could be used in combination to lyse tumor cells and prevent potential off-tumor toxicity.

Discussion

Here we describe the MICS system which has the potential to overcome limitations of current multiparametric technologies and to complement single cell experiments. As the tissue samples are left

intact, MICS allows the combination with other technologies and thereby provides a first step for high context single cell analyses for basic research and the basis for high context single cell analyses for pathology in an regulated environment. By using fluorescently labelled binders and a gentle signal erasure we combine the advantage of direct highly sensitive fluorescent imaging with subcellular resolution and the ability to apply more than 300 binders to the same specimen.

Mass spectrometry is limited by the number of transition element isotopes[3] and existing cyclic immunofluorescent approaches are limited as they either apply all antibodies at once and have a secondary oligonucleotide-based readout and/or use harsh and complex chemistry, i.e. peroxides for signal bleaching, antibody crosslinking chemistry, or oligonucleotide hybridization[5,9]. Our directly conjugated binders circumvent the need to control and quantify a secondary binding step as secondary antibodies or oligonucleotides and antibody panels can be arranged in a flexible way. We report a sensitivity aqivalent to about 11 proteins per cell and a high degree of linearity over five orders of magnitude. This is similar to what has been reported for super resolution microscopy[20]. Sensitivity and specificity to detect rare cells is also increased by multiplexing and allows to detect rare cells limited only by the total number of cells recorded. The high reproducibility of our approach is reflected by the possibility to restain the same epitope (Fig S1).

A common problem with multiparametric analysis is the complexity of handling hundreds of binders and the duration per experiment. We address the complexity by automating the process and reduce the processing time by selecting for binders qualified for sensitivity, specificity and a short reaction time of 10 min. The signal erasure is roughly 10 min and with an image acquisition time of 10 min this sums up to roughly 20 h for a typical experiment with 100 antibodies. This will be further reduced by increasing the image acquisition speed and the number of fluorescence channels.

Targeted immunotherapy has achieved clinical benefits for patients in recent years[21,22]. A potential threat is still on-target/off-tumor toxicity[23,24]. Currently, most prediction methods for on-target/off-tumor expression are based on mRNA expression data. These prediction models, however, have limitations, mainly due to poor correlation between RNA and protein expression levels. Multiple targeting of different antigens is supposed to reduce the risk of on-target/off-tumor toxicity employing cell therapies like CAR T cells[25]. We introduce MICS as a pre-clinical assay and suggest target pairs for GBM, HGSOC, and PDAC in comparison to unaffected tissue including the co-expression of THY1 and EPCAM on ovarian cancer cells in a subset of HGSOC but not on unaffected tissue. *In vitro* validation with adapter CAR T cells for an AND gated targeting shows efficient killing of double positive cells only. While this is a promising approach to reduce potential toxicity of CAR T cells it also reduces the coverage of cancer cells and thereby increases the risk of tumor escape. However, the adapter CAR technology opens the possibility to treat multiple targets and target pairs sequentially and here again MICS as an efficient multiparametric analysis of patient material will be instrumental in guiding the choice of targets.

Methods

Tissues, PBMCs, Cell lines and culture conditions

High grade serous ovarian cancer patient samples were provided by Prof. Dr. Peter Mallmann (Department of Obstetrics and Gynecology Medical Faculty, University of Cologne), pancreatic ductal adenocarcinoma were provided by Prof. Dr. Philipp Stroebel (Institute of Pathology, University Medical Center Göttingen), and glioblastoma samples were provided by Prof. Dr. med. Wolfgang Brück (Institute for Neuropathology, University Medical Center Göttingen) or purchased from BioIVT and used with informed consent by the patients. Fresh frozen healthy organ tissue samples were purchased from BioIVT and ProteoGenex. All pancreatic ductal adenocarcinoma (PDAC) patient derived xenografts (PDX) were obtained from Charles River Discovery Research Services Germany GmbH.

The mouse frozen embedded tissue section is derived from a frozen C57BL/6 mouse spleen provided by the Czech Centre for Phenogenomcis by PD Dr. rer. nat. Radislav Sedlacek and is part of a control group of a bigger experiment characterising mouse mutants using the MICS system which will be published spearately.

Buffy coats and leukaphereses were obtained from the University Hospital in Cologne and Dortmund. Peripheral blood mononuclear cells (PBMCs) were isolated from buffy coats by density gradient centrifugation. Before imaging, PBMCs were washed 3x in PBS and transferred to multiple wells of a glass-bottomed (170 µm coverslip) 24-well plate (with $1x10^6$ PBMCs /well). They were then centrifuged at 1000xg for 10 min (RT), fixed for 10 min using 4% paraformaldehyde (PFA), and finally washed (3x) with PBS buffer.

HEK293T and A2780 cells were purchased from American Type Culture Collection (Manassas, VA) and cultured in DMEM (Biochrom, Nuaillé, France) supplemented with 2 mM glutamine (Lonza, Basel, Switzerland) and 10% FCS (Biochrom, Berlin, Germany). Cell confluency ranged typically between 20–80% during the culture maintenance phase. All human primary cellular products were derived from healthy donors after informed consent and cultivated in TexMACS medium (Miltenyi Biotec, Bergisch Gladbach, Germany) following processing.

Flow cytometry

Tissue were dissociated using the Tumor Dissociation Kit, human in combination with the gentleMACS™ Octo Dissociator with Heaters (both Miltenyi Biotec). When processing PDX models, mouse cells were depleted using the Mouse Cell Depletion Kit (Miltenyi Biotec). Resulting cell suspensions were analyzed using the MACS® Marker Screen, human (Miltenyi Biotec) a monoclonal antibody panel containing 371 pre-titrated antibodies with 9 isotype controls, or candidate antibodies selected from this panel for subsequent screening steps. All samples were measured on MACSQuant® Analyzer and analyzed using the MACSQuantify™ Software or FlowJow v10.7.1.

Tissue processing for microscopy

Frozen embedded tissue specimen were cryosectioned with a CM3050 cryostat (Leica), 8 µm sections were mounted on SuperFrost® Plus slides (Menzel). For acetone fixation the sections were fixated in -20°C cold acetone for 3 minutes prior to the slide storage at -80°C. On the day of use, the slide was immerged into in -20°C cold acetone for 10 minutes for thawing. After short air drying the appropriate MACSWell™ imaging frame was mounted immediately on the slide and the appropriate initial sample volume of MACSima Running Buffer was added (according to the MACSWell™ imaging frames datasheet). For paraformaldehyde (PFA) fixation, the cryosectioned slices on slides were directly stored at -80°C. On the day of use, the frozen slide was put in a 4% PFA solution and incubated for 10 minutes at room temperature. The slide was washed three times with MACSima Running Buffer. After washing the appropriate MACSWell™ imaging frame was mounted immediately on the slide and the appropriate initial sample volume of MACSima Running Buffer was added (according to the MACSWell™ imaging frames datasheet). Right before the start of the MACSima ^{TM} instrument a DAPI pre-staining was performed: the MACSima Running Buffer was removed from the sample to be analysed and stained for 10 min with a 1:10 dilution of a DAPI staining solution (volume depends on working volume for the different MACSwell™ formats, see datasheet). The DAPI staining solution was removed and 3 washing steps were performed (MACSima Running Buffer). Finally, the initial sample volume of MACSima Running Buffern was added.

Antibodies and conjugates for microscopy

The following three types of reagents were used in this work for iterative staining and imaging with MACSima: Fluorescently labelled antibodies, REAdyelease and REAlease staining reagents. Fluorescent antibodies were prepared by chemical linking of one or more fluorescent dyes to a corresponding recombinant (REAfinity™) antibody. Recombinant antibodies are derived from a defined set of genes, ensuring the consistency in antibody structure and performance. A typical example of recombinant fluorescent antibody used in this work is CD4-FITC (CD4 Antibody, anti-human, FITC, REAfinity™, 130-114-531). REAdyelease reagents were prepared by covalent linking and fluorescent labelling of two or more antibody fragments. The chemical linker between the antibody fragments and fluorescent dyes can be disrupted by a specific releasing reagent leading to release of fluorescent dyes and resulting in erase of fluorescence staining. A typical example of REAdyelease conjugate used in this work is CD11c-PE (CD11c Antibody, anti-human, PE, REAdye_lease™ 130-121-314). REAlease reagents were prepared by covalent linking and fluorescent labelling of two or more antibody fragments that are characterized by low epitope binding affinities. Due to multimerization of antibody fragments, REAlease conjugates possess high-avidity and are comparable to conventional antibody-fluorochrome conjugates in terms of labeling properties. The chemical linker between the antibody fragments can be disrupted by a specific releasing reagent. This leads to monomerization of the antibody fragments and their dissociation from the epitope resulting in erase of fluorescence staining and availability of the epitope for restaining. Typical examples of REAlease conjugates used in this work are CD8-FITC (CD8 Antibody, anti-human, FITC, REAlease®, 130-112-070) and CD19-FITC (CD19 Antibody, anti-human, FITC, REAlease®, 130-112-073). To characterize the expression of proteins in the murine spleen and on on cancerous and healthy human

tissues antibody panels were designed. A list of all antibodies used in the respective experiment is given in Supplementary Table 1.

Cyclic immunofluorescence staining with the MACSima™ Imaging System

The MACSima™ Imaging System is a fully automated instrument combining liquid handling with widefield microscopy for cyclic immunofluorescence imaging. In brief, staining cycles consisted of the following automated steps: immunofluorescent staining, sample washing, multi-field imaging, and signal erasure (photobleaching or REAlease). Cyclic immunofluorescence with the MACSima is optimally applied on thin tissue cryosections (few micron thick), cultured cells, or suspension cells (either captured in microcavities or centrifuged down onto the glass). We developed MACSwell sample carriers specifically to provide the reaction cavities necessary to perform MICS experiments with the MACSima Imaging Platform. To support either tissue sections of varying size or adherent cells we designed different kinds of sample carriers: MACSwell One, Two, and Four Imaging Frames, and MACSwell 24 Imaging Plates.

Liquid Handling: The liquid handling system is comprised of a syringe pump, peristaltic pumps, a valve head, tubing, and a robotic needle. The valve head connects the needle with the externally mounted buffer bottles (MACSima™ Running Buffer, MACSima™ Storage Solution, MACSima™ System Buffer) and the waste bottle. The valve head allows for switching of the syringe pump to each of the bottles and the needle. To avoid carryover between pipetting steps, needle washing is performed by flushing the needle from both inside and outside with fresh buffer. Additional peristaltic pumps transport the used fluids to the waste bottle. An internal reagent bank has positions for other reagents that can be accessed with the needle (e.g. DAPI, FcR block, REAlease™ Release Reagent). The liquid handling system automates in particular the following steps: (1) preparation of the antibody conjugate staining solution (e.g. resuspension of dried antibody conjugates, dilution/mixing of conjugates), (2) application of the staining solution or the REAlease™ Release Reagent to the biological sample residing in a specific well of a disposable sample plate, and (3) sample washing following the staining or release incubation steps.

Microscope: All microscope images on the MACSima are obtained using an epifluorescence setup with one of three different objectives: 20x objective (NA 0.75, 170-micron coverslip glass), long-working-distance 20x objective (NA 0.45, objective slides 1.0 mm), and 2x (NA 0.1). Fluorescence excitation is achieved with custom-designed illumination based on a set of LEDs (infrared, red, green, blue, UV) with LED-specific filters to narrow the excitation light spectrum. Additional excitation/dichroic/emission filter sets define the epifluorescence channels optimized for standard dyes (e.g. DAPI, FITC, PE, APC, and Vio780). Images are captured by a monochromatic scientific CMOS (SCMOS) camera with 106 nm/pixel for the 20x objectives and 1060 nm/pixel for the 2x objective. Autofocusing is achieved in two ways. A hardware autofocus measures the position on the glass surface using infrared light to a precision of < 1 µm. Image-based autofocusing is also possible via optimization of the DAPI image.

Photobleaching: Photobleaching is achieved by focusing an additional set of red, green, and blue LEDs onto a single square spot (3 mm x 3 mm). Illumination with the blue LED (2 W/cm^2 at the sample; 2 min), green LED (0.4 W/cm^2 at the sample; 2 min) or red LED (1 W/cm^2 at the sample; 6 min) led to a > 90% reduction of the FITC, PE or APC intensity.

Stage: Reagent plates and sample holders are mounted on an xy-stage (with positional accuracy on the order of a few µm) to align the biological sample with the optical path of the microscope or with the photobleaching position, as well as to bring the reagents and sample to the needle position.

Image Acquisition and Processing: The image processing pipeline for the MACSima is displayed in Fig. S2. In the first step, a series of single-channel exposures of a fixed position in the sample are combined into a single, statistically optimal, high dynamic range (HDR) image based on a calibrated Gaussian noise model for the IRIS 15 SCMOS camera. Our use of an HDR representation for the images allows for the removal and replacement of all saturated pixels and additionally boosts signal-to-noise in the dimmer portions of the image. In the next steps, the HDR image is corrected in each pixel for the sensor flatfield (pixel-to-pixel differences in quantum efficiency), the optical profile (illumination/detection gradient across the field of view), and hot/cold outlier pixels (by median filtering). Non-local corrections are then performed over the image to correct for distortion (including chromatic effects), to register the images over the cycles, to stitch neighboring (overlapping) images together, and to downsample to the Nyquist frequency. Spectral unmixing of the image (along with corresponding images obtained for the other channels) is then performed based on a calibrated crosstalk matrix. A final subtraction of the pre-stain image removes any residual intensities from remaining autofluorescence or incomplete erasure of the previous cycle staining. While not all images presented in this publication were analyzed with the full pipeline as described above, the most critical processing steps corresponding to the removal of saturated pixels, replacement of hot/cold pixels, flatfielding, and subtraction of the pre-image were applied to all data sets presented here. Further details of the image processing pipeline will appear in a separate publication.

Image Analysis

Image data sets (stack of images) for each tissue were imported into the software QiTissue™. The software uses nuclei and cell membrane markers to perform image segmentation identifying individual cells. As it uses all the cell membrane markers known to the QiTissue™ system simultaneously, it can segment most types of cells in a sample. For each tissue similar segmentation parameters were used. Once the cells are identified, the features like mean fluorescent intensities (MFI) are computed for each cell against the background. These intensities are then used for further downstream processing. During the downstream analysis, all computed MFI are scaled between the range 0 and 1 for visualization and comparability.

Bead Experiments

Fluorophore-labeled beads were used to compare the linearity and sensitivity of image cytometry by the MACSima with flow cytometry by the MACSQuant in the following way. Compensation beads from the MACS Compensation Bead Kit, anti-REA (130-104-693) were incubated with different stoichiometric mixtures of CD4-APC (130-113-222) and dark CD4-Biotin (130-113-224) antibodies (clone REA623). The anti-REAfinity antibody conjugated to the bead surface generically recognizes Miltenyi REAfinity antibodies through their kappa light chains, with the specific CD4-recognition domain here playing no role. Saturation of CD4-APC antibodies on the beads was determined from a titration series to occur at roughly 10 µg/mL (95% saturated). Compensation beads were diluted (1:2) and incubated in the dark (10 min, RT) in MACSQuant Running Buffer (130-092-747) to a final volume of 400 µL with stoichiometric mixtures of CD4-APC to CD4-Biotin antibodies at overall saturating conditions equivalent to the following percentages of labeled probe: 100, 10, 1, 0.33, 0.10, 0.030, 0.010, 0.0030, 0.0010 (see Fig. 2a). Samples were shaken during incubation and diluted afterwards with 1 mL of the buffer to stop the incubation process. The beads were then centrifuged at 300xg for 5 min to remove unbound antibodies and washed 1x in the original volume of 400 µL. Half of the volume of each of the samples was transferred to a well of a glass-bottomed (170 µm coverslip) 24-well plate (~ $1x10^6$ beads/well) for image cytometry with the MACSima and the other half was used for flow cytometry with the MACSQuant.

For flow cytometry by the MACSQuant, beads were gated in the software MACSQuantify v.2.13.0 using the following gating strategy. (1) Draw an ellipse gate around the densest region of beads in a FSC-A vs. SCC-A density plot (A = area of detection peak, FSC = forward scatter, SSC = side scatter). (2) Draw a polygon gate around the linear fit events in an FSC-A vs. FSC-H plot (H = height of peak) to purify for singlets. (3) Draw an interval gate around the bead distribution in an APC-A histogram plot.

For image cytometry of the beads by the MACSima, fifteen separate positions in each well were imaged (see cropped example image in Fig. 2a inset) with the images spaced far enough apart (by 1 mm) from one another to avoid inter-image photobleaching during acquisition. Several hundred beads were acquired per position with, consequently, several thousand total beads imaged for each well (each assayed percentage, see Fig. 2a). Imaging consisted of an exposure series (60, 160, 640 ms) in the APC channel (total acquisition photobleaching was < 5%) followed by a single exposure (1500 ms) in the DAPI channel of the weak bead autofluorescence, with the latter image used to create masks around each detected bead that were therefore independent of the degree of APC staining.

The brightest unsaturated image in each APC channel image series was processed in the following way: (1) Subtract camera readout offset. (2) Flatfield by dividing by a readout-offset-subtracted image of APC in solution. (3) Divide by exposure time.

For object mask creation, the bead autofluorescence image was analyzed in ImageJ/FIJI as follows: (1) Subtract camera readout noise. (2) Perform Gaussian blur with σ = 3 pixels. (3) Perform “Auto Local Threshold” with “Median” filter and radius = 15 pixels to obtain binary image. (4) From “Morphological Filters”, dilate as a disk with radius = 2 pixels. (5) Fill holes. (6) Perform watershed. (7) Label all particles

with area greater MIN = 4000 and less than MAX = 12000 pixels, and with circularity greater than 0.1. (8) Save object masks.

To remove background in the APC channel from the object mask pixels, the background was interpolated in the following way: (9) Return to the mask resulting from “(5) Fill holes” above. From “Morphological Filters”, dilate as a disk with radius = 17 pixels and then invert to create a mask for the background. (10) Mask the processed APC channel image to reveal only pure background regions. (11) Using a custom-written Python routine, place a uniform grid (with non-overlapping quadrants of size 400x400 pixels) over the background image (5056x2960 pixels) to downsample it by performing a median filter over each quadrant with assignment of the median value to the central position of each quadrant. (12) In Python, interpolate over the median values (quadrant centers) to estimate the background contribution to the object mask pixels using “griddata” (OpenCV) with the method “cubic” for bulk pixels followed by the method “nearest” for boundary pixels. (13) In ImageJ, subtract interpolated background image from the initial processed APC channel image. (14) Integrate background-subtracted bead intensities over each object mask and save the results as a table.

PBMC Experiments

To compare the sensitivity of MACSima image cytometry with MACSQuant flow cytometry on a real biological sample, peripheral blood mononuclear cells (PBMCs) were examined as follows. A buffy coat from a healthy anonymous donor was obtained from the German Red Cross Dortmund, and the PBMCs were isolated by density gradient centrifugation. The cells were stained with CD45-VioBlue (130-110-637) as a general marker for PBMCs and were additionally stained with different stoichiometric ratios of a fluorescent CD3-APC antibody (130-113-135) and a non-fluorescent CD3-Biotin antibody (130-113-137). More specifically, a 1.5 mL suspension of fresh PBMCs containing $2x10^7$ cells/mL was prepared using autoMACS Running Buffer (130-091-221). Furthermore, buffer was added to separate Eppendorf tubes along with CD45-VioBlue (1:50) and mixtures of the CD3-APC and CD3-Biotin antibodies at the stoichiometries listed in Table 1 and at overall high saturation (the standard dilution of 1:50 for the CD3 antibodies implies a high degree of saturation of the targeted CD3 epitopes), considering a 1:3 cell suspension dilution and a final volume of 300 µL. Then, 100 µL of the prepared PBMC suspension was added to the 200 µL contained in each separate tube. Cells were stained in the dark and shaken during incubation (10 min, RT). Afterwards, samples were diluted with 1 mL of buffer to stop the incubation process. The cells were then centrifuged at 300xg for 5 min to remove unbound antibodies, resuspended in 200 µL of 4% paraformaldehyde (PFA) and fixed for 10 min in the dark. Subsequently, cells were centrifuged at 600xg (fixed cells are lighter) for 5 min to remove PFA, and washed 1x in 300 µL of buffer, with half (150 µL) used for MACSima image cytometry and the other half for MACSQuant flow cytometry.

For the MACSQuant, CD45 + cells were gated using density plots according to the following strategy. (1) Draw a polygon gate around the linear fit events in a FSC-A vs. FSC-H plot. (2) Disregard platelets, red blood cells, and debris (low FSC-A signals) with a rectangular gate drawn in a FSC-A vs. SSC-A plot. (3) Select CD45 + cells with a rectangular gate in a CD45-VioBlue-A vs. SSC-A plot. Then, assess the selected cells for their CD3-APC-A (integrated) intensities.

For the MACSima, 150 µL of the cell suspension from each tube was transferred to a well of a glass-bottomed (170 µm coverslip) 24-well plate and centrifuged at 100xg for 10 min to stick them to the bottom of the well. Image acquisition was identical to that used for the beads, with the exception that fewer cells were acquired per field. Image analysis was also largely identical to that used for the beads (see *Bead Experiments* above), aside from using the CD45-VioBlue staining to create the cell masks instead of autofluorescence, omission of the watershed, and allowance for objects with areas up to MAX = 15000 pixels. For both MACSQuant and MACSima datasets, the individual integrated cell intensities, *I*, were converted by the following formula to an arcsinh scale that is asymptotically equivalent to $\log_{10}$, but importantly also allows for negative values:

$y = \mathrm{arcsinh}(aI - b)/\ln(10)$,with the normalization factors *a* and *b* independently chosen for each dataset such that the mean (in arcsinh units) of the blank distribution equals 0 and the mean of the highest stained population equals 2 (see Fig. 2c).

Gene design

Gene synthesis in combination with an optimization algorithm for codon usage in humans (ATUM, Newark, CA) was used to design genes of interest. E. coli DH5alpha were used for cloning and plasmid generation. Plasmids were purified using DNA isolation kits (Quiagen).

Lentiviral vector production

Second generation self-inactivating VSV-G-pseudotyped lentiviral vectors were produced by transient transfection into adherent HEK293T cells. One day before transfection, $1.6x10^7$ HEK293T cells were seeded per T175 flask. Each T175 flask was then transfected with a total of 35 µg plasmid DNA composed of pMDG2 (encoding VSV-G), pCMVdR8.74 (encoding gag/pol), and the respective transgene-encoding transfer vector using MACSfectin reagent (Miltenyi Biotec). All transfection reactions were performed with a DNA:MACSfectin ratio of 1:2. Following overnight incubation, sodium butyrate (Sigma-Aldrich) was supplemented at a final concentration of 10 mM. After 48 hours the medium was collected, cleared by centrifugation at 300xg and 4°C for 5 min and filtered through 0.45 µm-pore-size PVDF filters. Concentration of the viral stock was performed by centrifugation at 4°C and 4,000xg for 24 hours. Pellets containing lentivirus were air-dried and resuspended at a 100-fold concentration with 4°C cold PBS. Lentiviral aliquots were stored at 80°C. In order to generate EPCAM positive A2780 cells human EPCAM lacking intracellular domains was cloned in the transfer vector. To generate eGFP positive A2780 cells a cassette containing eGFP was cloned in the transfer vector.

Cell engineering

A2780 THY1 knockout cells were generated in-house by CRISPR/Cas9-mediated knockout and subcloning. The respective THY1 gRNA used was GACGAAGGCTCTGGTCCACT. A2780 cells were electroporated at a density of 10^5 cells/ml in a CliniMACS Prodigy electroporator. Ribonucleoprotein particle complexes were assembled according to the manufacturer's protocol (IDT).

Isolation of T cells and generation of CAR T cells

Peripheral blood mononuclear cells (PBMCs) were isolated from buffy coats or leukapheresis products by low-density centrifugation on Pancoll (Pan-Biotech, Aidenbach, Germany) and enriched for Pan T cells by negative magnetic selection (Miltenyi Biotec). The enriched Pan T cells were resuspended at a density of 1x106 cells/mL in TexMACS medium containing IL-7/15 and stimulated with T cell TransAct (all from Miltenyi Biotec). One day after activation, T cells were lentivirally transduced with a multiplicity of infection (MOI) of 1:5 with the respective concentrated vector. Cell numbers were determined every 2–3 days and fresh TexMACS medium supplied with IL-7/15 was added to maintain a cell concentration of 1x106 cells/mL until day 12. Analysis of CAR-expressing cells was routinely performed on day 6 after activation using flow cytometry and CAR detection via Biotin-PE. Afterwards, cells were expanded in the presence of IL-7/15until downstream processing.

CAR T cell killing assays

All functionality assays were performed with CAR T cell populations on day 12–14 following T cell TransAct activation and in TexMACS medium without additives. The frequency of CAR-expressing T cells was equalized before all functional assays and untransduced T cells served as a control for allogeneic reactivity. To analyze CAR T cell-mediated cytotoxicity by target cell death, real-time monitoring using the IncuCyte S3 system (Essen BioScience, Ann Arbor, MI) was performed. Target cells were harvested using Trypsin (3min, 37°C) and cell numbers as well as target expression (THY1 REA897-APC, EPCAM REA764-Vioblue; staining was performed according to the manufactures protocol) were determined at MACS Quant 10. Afterwards target cells were seeded to ensure proper target cell adherence.

Assays were set up by seeding 25,000 GFP-transgenic target cells per well of flat bottomed 96 well plates and – following overnight incubation – adding CAR T cells to the cultures at a 1:2 (E:T) ratio. Subsequently, adapter molecules (THY1 REA897-Biotin, EPCAM REA764-Biotin) were supplemented at varying doses. Cultures of target cells only, target cells with mock-transduced T cells, and target cells with adapter CAR T cells without adapter molecule or unspecific adapter molecule were used as controls. Phase contrast and green fluorescence images were captured with 10x magnification every two hours for 3–6 days. Analysis of images was performed using the software provided by the manufacturer.

Ethics

For all studies using human primary tissue from glioblastoma, ovarian or pancreatic cancer, written informed consent was obtained following the guidelines of the approved Universitätsmedizin Göttingen, and Cologne Review Board protocol, respectively.

Peripheral blood mononuclear cells (PBMCs) were isolated from buffy coats of healthy anonymous volunteers that were purchased from the German Red Cross Dortmund. All blood samples were handled following the required ethical and safety procedures.

All animal experiments were approved by the Governmental Review Committee on Animal Care in NRW, Germany and performed according to guidelines and regulations. Animals were maintained under specific pathogen-free conditions according to the recommendations of the Federation of European

Laboratory Animal Science Association. All procedures were carried out in accordance with the European Communities Council Directive European Communities Council (86/609/EEC) and (2010/63/EU).

Healthy whole blood samples were taken from voluntary healthy donors that gave their written consent before.

Declarations

Acknowledgements

We want to thank Peter Mallmann, Philipp Stroebel, and Wolfgang Brück for their help and advice concerning the selection of tumor material, Radiskav Sedlacek for the mouse spleen sample, Sven Hensler for help in the description of the image processing pipeline, Florian Bohnensack for software scripting, and Karolina Schlegel for excellent technical assistance.

Author contributions

A.K., C.H., D.Y., W.M. and A.B. wrote the manuscript. A.K., C.H., D.Y., W.M., O.H., D.E., M.J., C.D. and A.B. designed the study. S.R., D.S., S.Re., and V.D. conducted experiments for target discovery. A.K., L.M., C.R., A.D., S.R. and J.P. generated antibody fluorochrome conjugates and/or performed experiments on fluorophore signal erasure. A.K., F.C.R. and M.B. planned, executed, and analyzed the linearity and sensitivity experiments of MICS vs. MACSQuant flow cytometry. P.P., J.Ko., M.N. and W.M. did the bioinformatical analysis. S.B., J.K., E.S., R.P.P. and S.M. engineered the instrument. M.MO. performed in vitro assays. T.D.R., S.M., J.S., R.P.P. W.M. and A.B. supervised the project. All authors discussed the data and reviewed the manuscript.

References

1. Schubert, W. *et al.* Analyzing proteome topology and function by automated multidimensional fluorescence microscopy. *Nature Biotechnology* **24**, 1270–1278 (2006).
2. Hennig, C., Adams, N. & Hansen, G. A versatile platform for comprehensive chip-based explorative cytometry. *Cytometry A* **75**, 362–370 (2009).
3. Bendall, S. C. *et al.* Single-cell mass cytometry of differential immune and drug responses across a human hematopoietic continuum. *Science* **332**, 687–696 (2011).
4. Rimm, D. L. Next-gen immunohistochemistry. *Nat Methods* **11**, 381–383 (2014).
5. Lin, J.-R., Fallahi-Sichani, M. & Sorger, P. K. Highly multiplexed imaging of single cells using a high-throughput cyclic immunofluorescence method. *Nat Commun* **6**, 8390 (2015).
6. Tsujikawa, T. *et al.* Quantitative Multiplex Immunohistochemistry Reveals Myeloid-Inflamed Tumor-Immune Complexity Associated with Poor Prognosis. *Cell Rep* **19**, 203–217 (2017).

7. Goltsev, Y. *et al.* Deep Profiling of Mouse Splenic Architecture with CODEX Multiplexed Imaging. *Cell* **174**, 968-981.e15 (2018).
8. Manesse, M., Patel, K. K., Bobrow, M. & Downing, S. R. The InSituPlex® Staining Method for Multiplexed Immunofluorescence Cell Phenotyping and Spatial Profiling of Tumor FFPE Samples. *Methods Mol Biol* **2055**, 585–592 (2020).
9. Schürch, C. M. *et al.* Coordinated Cellular Neighborhoods Orchestrate Antitumoral Immunity at the Colorectal Cancer Invasive Front. *Cell* **183**, 838 (2020).
10. Guedan, S., Ruella, M. & June, C. H. Emerging Cellular Therapies for Cancer. *Annu Rev Immunol* **37**, 145–171 (2019).
11. Li, J. *et al.* Chimeric antigen receptor T cell (CAR-T) immunotherapy for solid tumors: lessons learned and strategies for moving forward. *J Hematol Oncol* **11**, 22 (2018).
12. Hegde, M. *et al.* Combinational targeting offsets antigen escape and enhances effector functions of adoptively transferred T cells in glioblastoma. *Mol Ther* **21**, 2087–2101 (2013).
13. Wood, J. C. Fundamental flow cytometer properties governing sensitivity and resolution. *Cytometry* **33**, 260–266 (1998).
14. Hoffman, R. A. & Wood, J. C. S. Characterization of flow cytometer instrument sensitivity. *Curr Protoc Cytom* **Chapter 1**, Unit1.20 (2007).
15. Tabula Muris Consortium *et al.* Single-cell transcriptomics of 20 mouse organs creates a Tabula Muris. *Nature* **562**, 367–372 (2018).
16. Motomura, K. *et al.* Immunohistochemical analysis-based proteomic subclassification of newly diagnosed glioblastomas. *Cancer Sci* **103**, 1871–1879 (2012).
17. Schäfer, D. *et al.* Identification of CD318, TSPAN8 and CD66c as target candidates for CAR T cell based immunotherapy of pancreatic adenocarcinoma. *Nat Commun* **12**, 1453 (2021).
18. Arndt, C. *et al.* Adaptor CAR Platforms-Next Generation of T Cell-Based Cancer Immunotherapy. *Cancers (Basel)* **12**, (2020).
19. Grote, S. *et al.* Adapter chimeric antigen receptor (AdCAR)-engineered NK-92 cells: an off-the-shelf cellular therapeutic for universal tumor targeting. *Oncoimmunology* **9**, 1825177 (2020).
20. Nerreter, T. *et al.* Super-resolution microscopy reveals ultra-low CD19 expression on myeloma cells that triggers elimination by CD19 CAR-T. *Nat Commun* **10**, 3137 (2019).
21. Tan, S., Li, D. & Zhu, X. Cancer immunotherapy: Pros, cons and beyond. *Biomed Pharmacother* **124**, 109821 (2020).
22. Riley, R. S., June, C. H., Langer, R. & Mitchell, M. J. Delivery technologies for cancer immunotherapy. *Nat Rev Drug Discov* **18**, 175–196 (2019).
23. Neelapu, S. S. Managing the toxicities of CAR T-cell therapy. *Hematol Oncol* **37 Suppl 1**, 48–52 (2019).
24. Fisher, J. *et al.* Avoidance of On-Target Off-Tumor Activation Using a Co-stimulation-Only Chimeric Antigen Receptor. *Mol Ther* **25**, 1234–1247 (2017).

25. Jaspers, J. E. & Brentjens, R. J. Development of CAR T cells designed to improve antitumor efficacy and safety. *Pharmacol Ther* **178**, 83–91 (2017).
26. Bikoue, A. *et al.* Quantitative analysis of leukocyte membrane antigen expression: normal adult values. *Cytometry* **26**, 137–147 (1996).

Figures

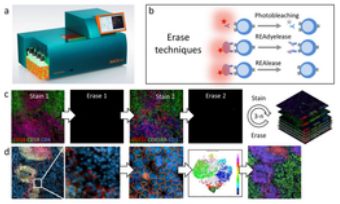

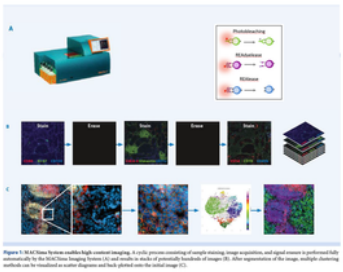

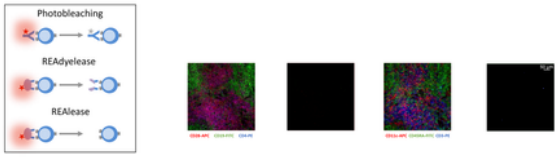

Figure 1A,B,C

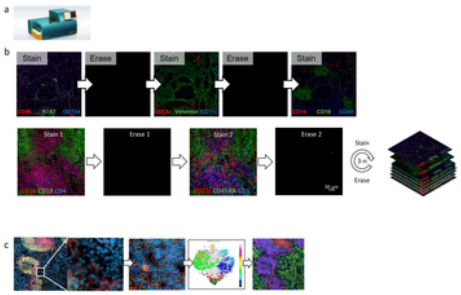

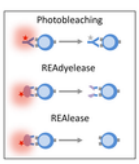

Figure 1

Cyclic Imaging with the MACSimaTM Imaging Platform. (a) MACSimaTM instrument with fully automated robotic liquid handling and microscopic acquisition. (b) Erase techniques based either on dye photobleaching, or disruption of the labeling conjugate by release reagent. The release reagent leads to a rapid detachment of the fluororecent dye only (REAdylease), or disruption of the labeling conjugate with a spontaneouse dissociation of the monomerized antibody fragments and the fluororecent dye (REAlease®) from their target epitopes. (c) Cyclic imaging. (d) Image analysis with QiTissue consisting of cellular segmentation, clustering, and visualization of clustered cells across the original image.

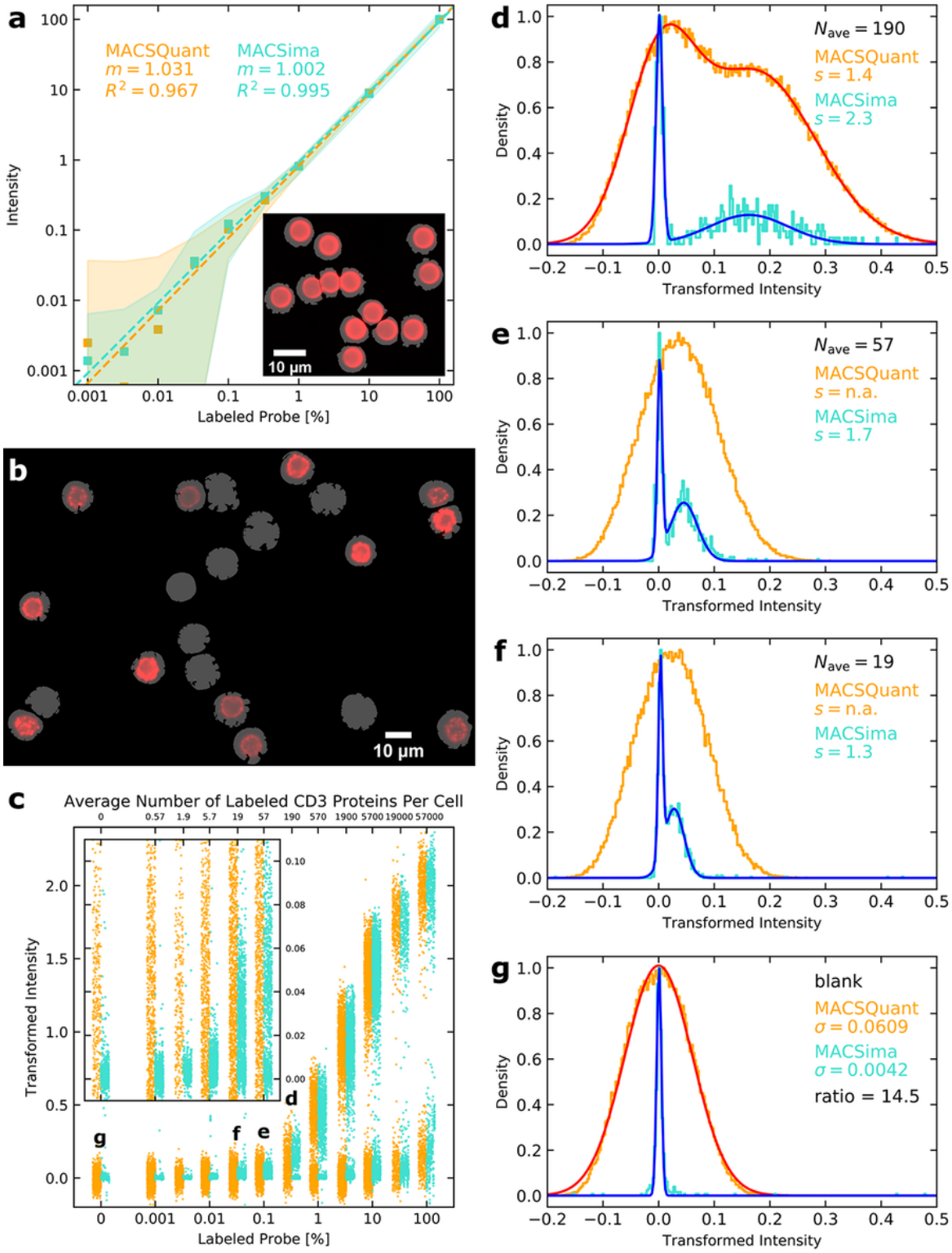

Figure 2

Comparison of linearity and sensitivity of MACSima image cytometry with MACSQuant flow cytometry. (a) Means (square symbols) and ± 1σ ranges (shaded regions) describing the population distributions for beads incubated with different percentages of APC-labeled vs. unlabeled antibodies by the MACSQuant (orange) and MACSima (cyan). For the MACSima images (see inset), bead autofluorescence in the DAPI channel was used to create individual bead masks (gray) over which the total background-subtracted

APC signal could be determined. Least-squares line fits on the log-log axes are shown (dashed lines), with the optimal slopes, m, and corresponding R2 values listed for each dataset. (b) MACSima image of PFA-fixed PBMCs labeled with a CD3-APC antibody (red) and a CD45-VioBlue antibody, with the latter staining used to generate the displayed masks (gray) for each CD45+ cell. (c) CD45+ PBMCs were assessed for their CD3-APC co-staining for different stoichiometric amounts of an APC-labeled vs. unlabeled CD3 antibody on the MACSQuant (orange) and MACSima cyan). The upper x-axis displays the approximate average number of labeled CD3 proteins per CD3+ cell for each assayed percentage, based on the average measured total copy number per cell of 5700026. Only a small representative subset of the full MACSQuant data (the latter ranging from 54581 to 167637 cells) is displayed for each assayed percentage of labeled probe to match the respective number of cells measured by the MACSima (ranging from 417 to 2384 cells). The inset gives a zoomed-in view of the y-axis for better visualization of the scatter plot distributions. (d-g) Histograms for specific assayed percentages of labeled probe are shown based on the complete datasets from both instruments. For Nave = 190 (d), the CD3+ cell population is recognizable in both datasets as a second peak, permitting a double Gaussian fit and consequent determination of the separation parameter, s. For Nave = 57 (e) and Nave = 19 (f), a second peak is only distinguishable in the MACSima dataset. The width of the distribution for the blank (g) provides a useful estimate of the measurement error expected for weak signals on both instruments.

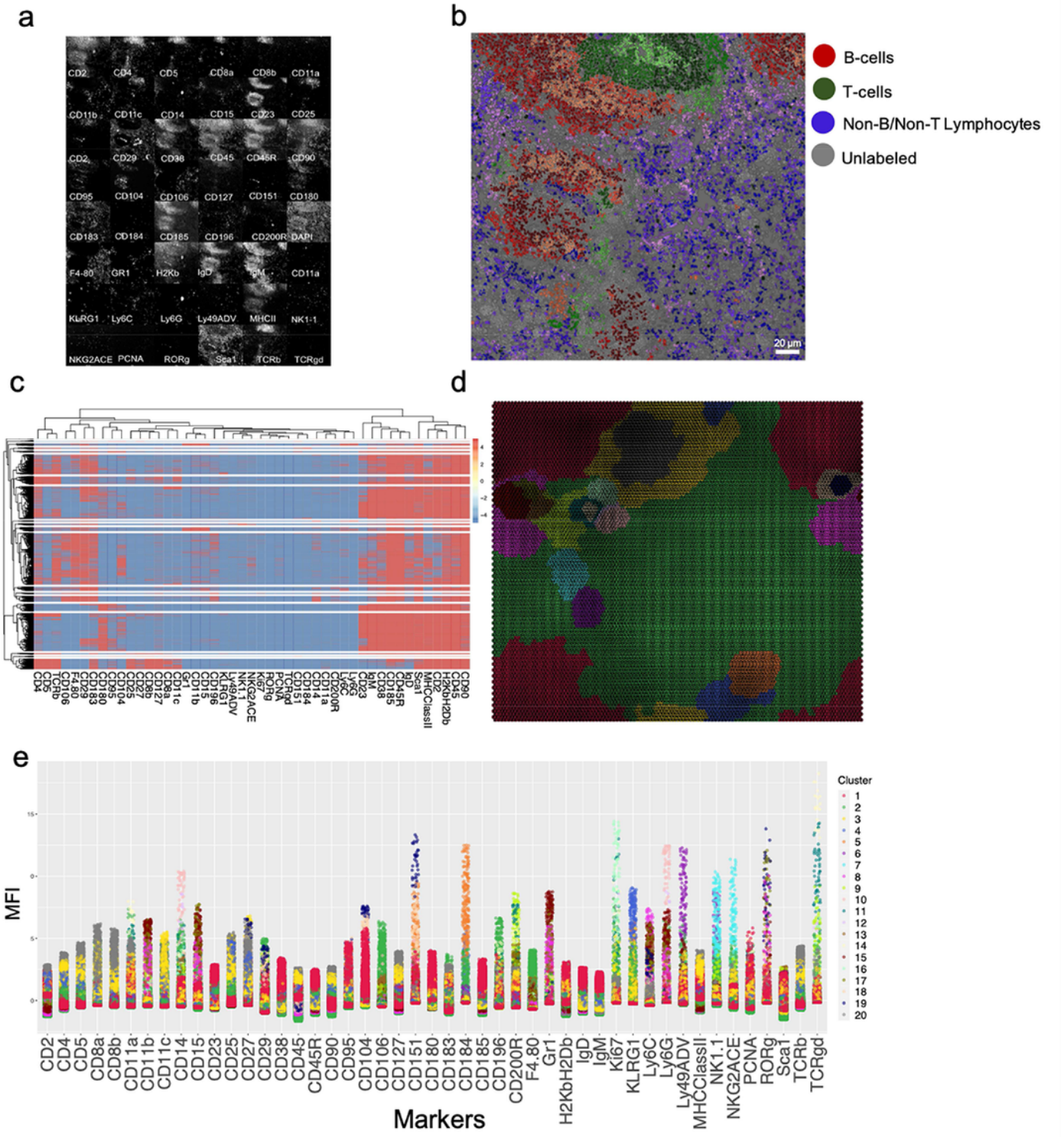

Figure 3

MACSima multi-channel analysis of a mouse spleen section A mouse spleen section was fixed by acetone and subsequently stained by directly fluorescently labeled antibodies in subsequent cycles. DAPI was used to stain the nuclei in the section, and it was used to register the images across the cycles and to segment the nuclei of the cells in the section. (a) small images of each of the channels used to generate the more complex data visualizations in the subsequent panels. In total 47 antibody staining and 1 DAPI

channel are shown. In panel (b) the result of an extensive k-means (40 clusters) clustering of the staining intensity values of cells after segmentation is shown, in which four cell populations are colored, B cells in red, T cells in green, and Non-B/Non-T cells in blue, and cells not recognized by the antibody panel in gray (17 clusters). The different color changes within the red (9 clusters), green (7 clusters) and blue (17 clusters) are subpopulations within the respective groups. Panels (c), (d) and (e) illustrate the results of hierarchical clustering (20 clusters) based on the mean staining intensity values of the cells. Panel (c) shows the marker expressions in the various subpopulations as defined by the hierarchical clustering in a heat map. Panel (d) shows the Kohonen map of the individual cell populations plotting induvial cells based on similarities. The color codes indicate the individual clusters based on the hierarchal clustering, with similar cells located closer. Panel (e) shows the marker expression of the individual cells and these are colored based on the hierarchical clusters.

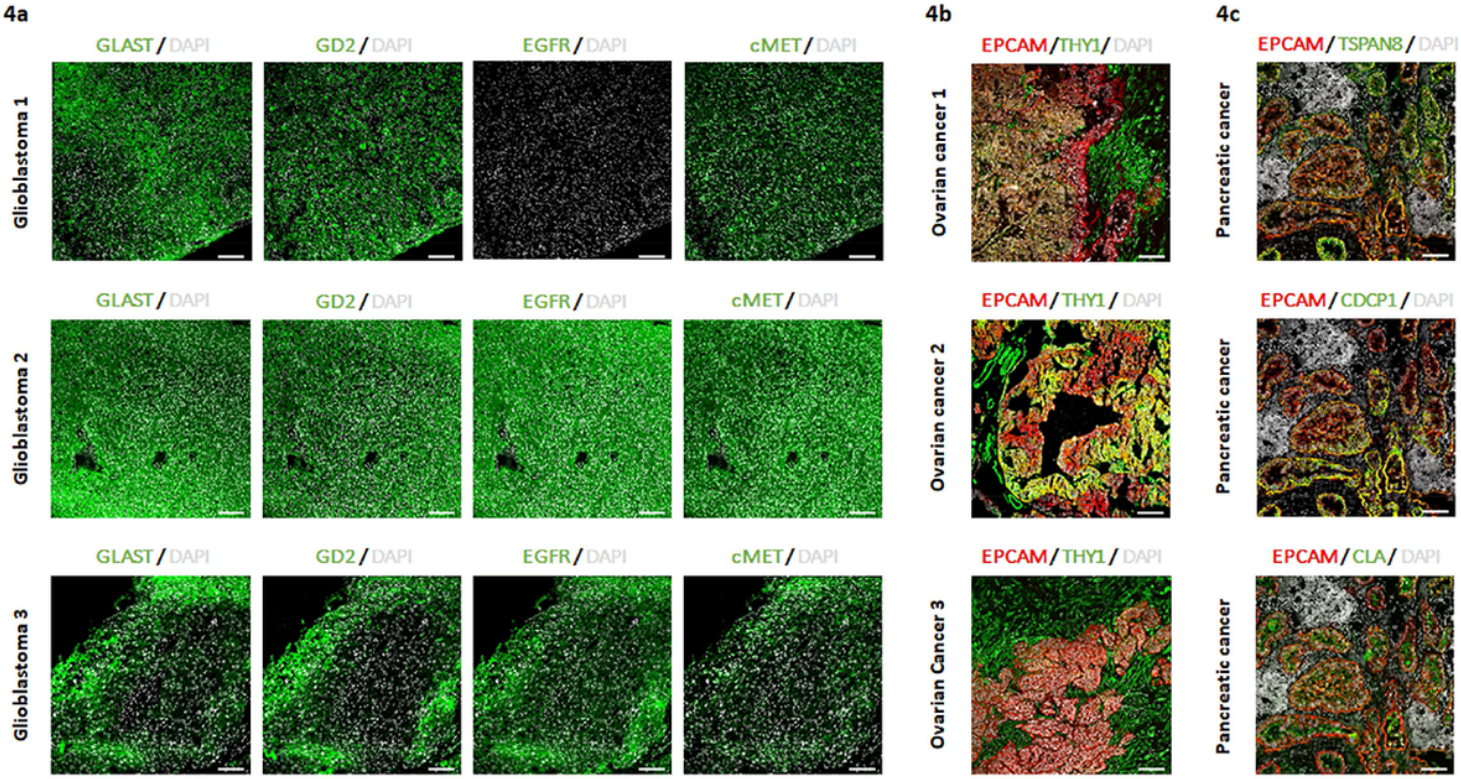

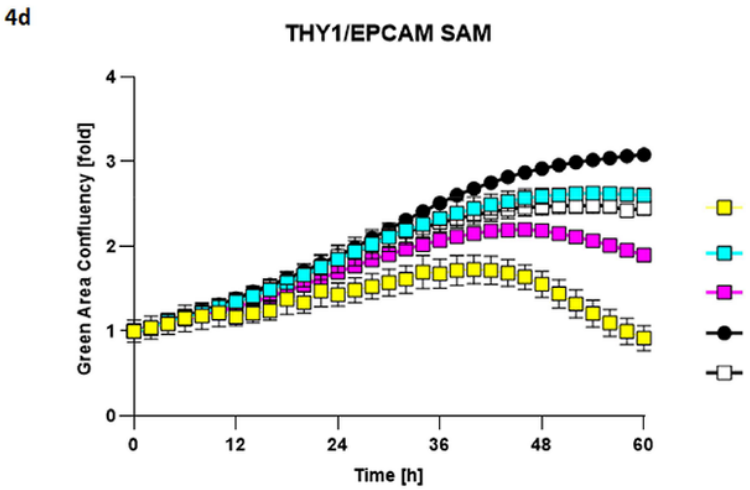

Target cells	Adapter CAR T cells	α-EPCAM-Biotin [ng/ml]	α-THY1-Biotin [ng/ml]
X	X	0.1	0.1
X	X	0.1	-
X	X	-	0.1
X	-	-	-
X	X	-	-

Figure 4

Ultra-high content imaging enables the discovery of novel targets and target pairs in different cancer indications which can be targeted and lysed in vitro by adapter CAR T cells. (a) - (c) Fresh-frozen human GBM, PDAC, and HGSOC samples were sliced and analyzed by MICS. DAPI is shown in white and the indicated markers of interest are shown in green or red. Scale bar represents 100µm. (a) Examples of MICS analysis of two GBM patient samples showing the expression of GD2, EGFR and cMET. (b) Example of a PDAC patient sample analysis displaying the co-expression of EPCAM (red) as a general epithelial and tumor cell marker with the potential PDAC marker candidates (green) TSPAN, CDCP1 and CLA. (c) Examples of three HGSOC samples. Sample 1 and 2 co-express EPCAM (red) and THY1 (green) while sample 3 expresses EPCAM but does not THY1. (d) Primary human T cells were isolated and transduced with a CAR construct against biotin. Anti-biotin CAR T cells were co-cultured with THY1-, EPCAM-, and GFP-expressing target cells for 72h in the presence of sub-optimal single adapter doses with the combinatorial use of sub-optimal adapter doses. GFP-fluorescence was measured over time. CAR T cell mediated lysis of target cells results in decreased GFP-fluorescence. Each data point represents mean of a technical replicate +/- SEM. Representative graph from n=3 experiments shown.

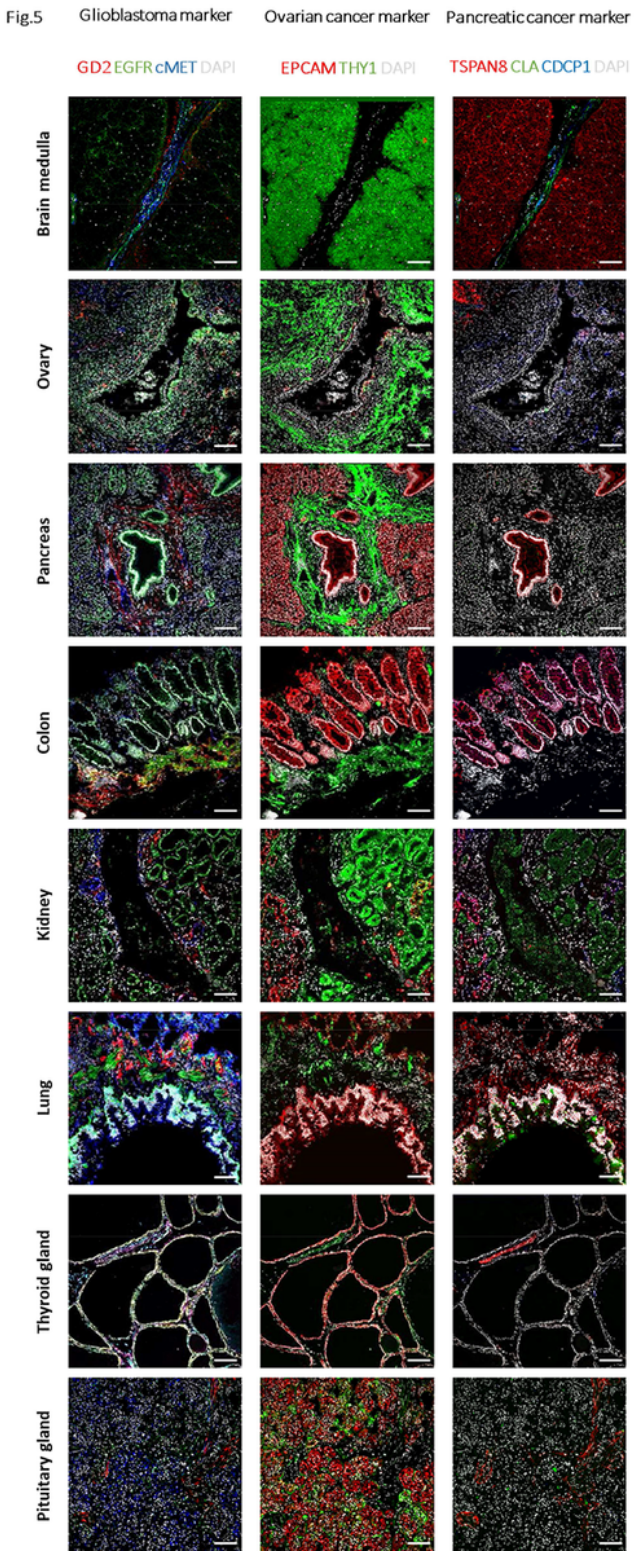

Figure 5

Ultra-high content imaging validates expression of target candidates on healthy human tissues to predict safety and toxicity of target candidates. Fresh-frozen human tissueswere sliced and fixed with acetone. The subsequent screening was performed on the MACSimaTM ultra-high-content imaging platform by employing a sequential staining of antibodies. Healthy human tissues, i.e. medulla oblongata, ovary, pancreas, colon, kidney, lung, thyroid gland, and pituitary gland, were analyzed for the expression of

glioblastoma target candidates (left panel), GD2 is shown in red, EGFR is shown in green, cMET is shown in blue, and DAPI is shown in white, respectively; ovarian cancer target candidates (middle panel), EPCAM is shown in red, THY1 is shown in green, and DAPI is shown in white, respectively; pancreatic cancer target candidates (right panel), TSPAN8 is shown in red, CLA is shown in green, CDCP1 is shown in blue, and DAPI is shown in white, respectively. Scale bar represents 100μm.

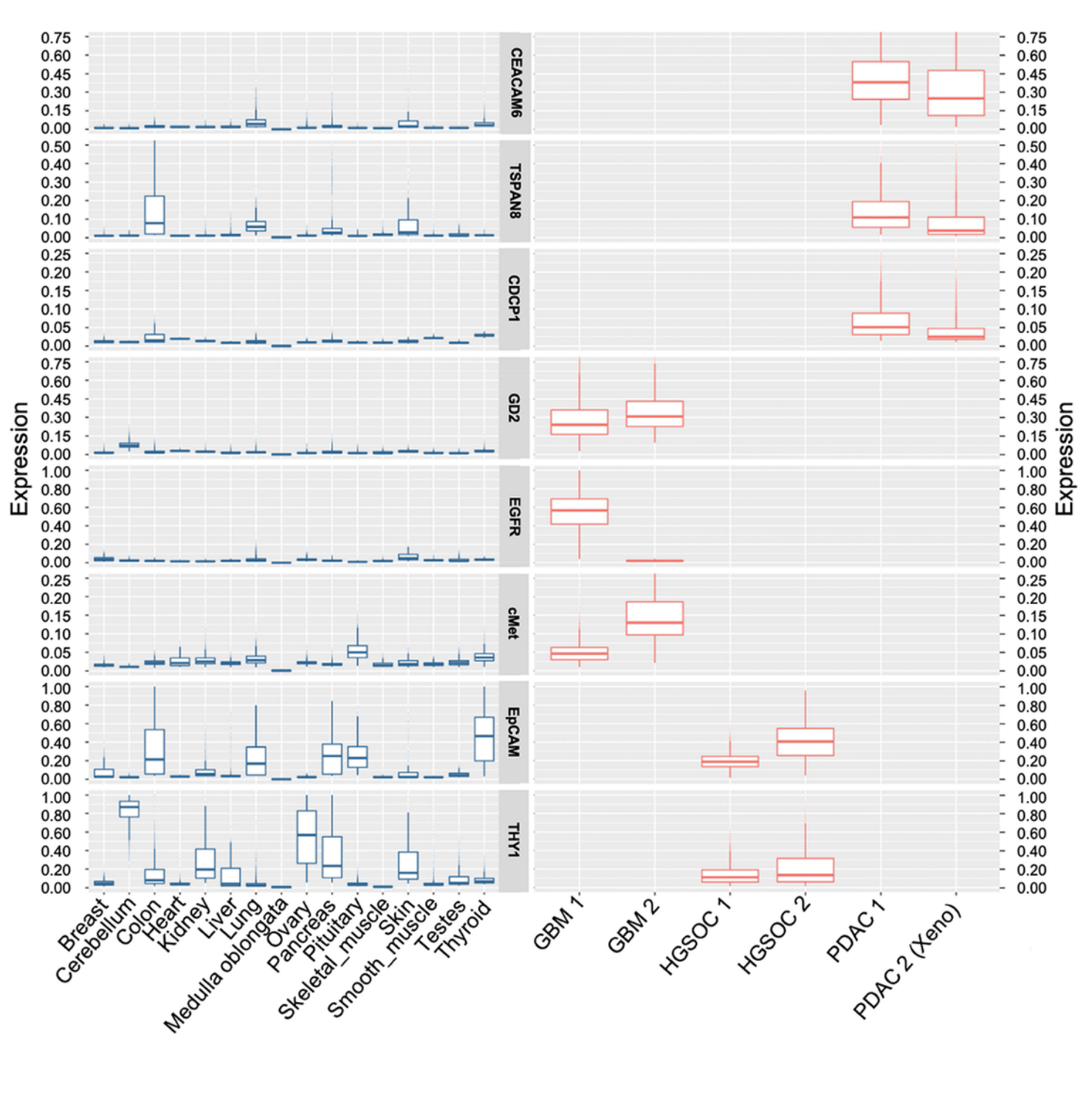

Figure 6

Comparison of marker expression in healthy and cancer samples Note indication of expression values only in tissue of interest

Supplementary Files

This is a list of supplementary files associated with this preprint. Click to download.

- MICSABosioSupplementaryinformation.pdf